Nanoscale

Accepted Manuscript

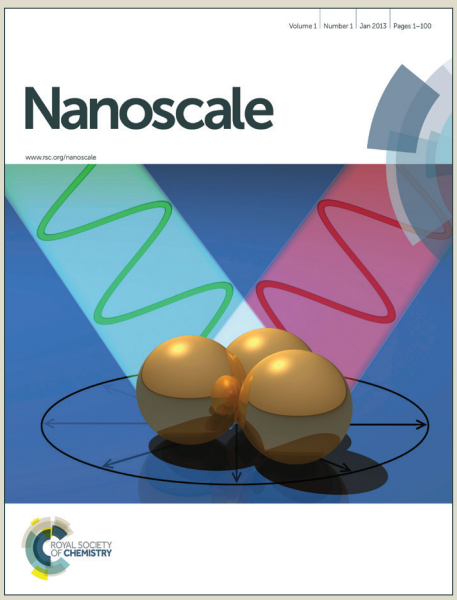

ROYAL SOCIETY OF CHEMISTRY

www.rsc.org/nanoscale

Journal Name

RSCPublishing

ARTICLE

Double Heterojunction Nanowire Photocatalysts for Hydrogen Generation

Cite this: DOI: 10.1039/x0xx00000x

P. Tongying,[a] F. Vietmeyer,[a] D. Aleksiuk,[b] G. J. Ferraudi,[c] G. Krylova*[d] and M. Kuno*[a]

Received 00th January 2012,
Accepted 00th January 2012

DOI: 10.1039/x0xx00000x

www.rsc.org/

Charge separation and charge transfer across interfaces are key aspects in the design of efficient photocatalysts for solar energy conversion. In this study, we investigate the hydrogen generating capabilities and underlying photophysics of nanostructured photocatalysts based on CdSe nanowires (NWs). Systems studied include CdSe, CdSe/CdS core/shell nanowires and their Pt nanoparticle-decorated counterparts. Femtosecond transient differential absorption measurements reveal how semiconductor/semiconductor and metal/semiconductor heterojunctions affect the charge separation and hydrogen generation efficiencies of these hybrid photocatalysts. In turn, we unravel the role of surface passivation, charge separation at semiconductor interfaces and charge transfer to metal co-catalysts in determining photocatalytic H_2 generation efficiencies. This allows us to rationalize why Pt nanoparticle decorated CdSe/CdS NWs, a double heterojunction system, performs best with H_2 generation rates of ~434.29 ± 27.40 μmol h^{-1} g^{-1} under UV/Visible irradiation. In particular, we conclude that the CdS shell of this double heterojunction system serves two purposes. The first is to passivate CdSe NW surface defects, leading to long-lived charges at the CdSe/CdS interface capable of carrying out reduction chemistries. Upon photoexcitation, we also find that CdS selectively injects charges into Pt NPs, enabling simultaneous reduction chemistries at the Pt NP/solvent interface. Pt nanoparticle decorated CdSe/CdS NWs thus enable reduction chemistries at not one, but rather two interfaces, taking advantage of each junction's optimal catalytic activities.

Introduction

Hydrogen is an attractive alternative to fossil fuels that can help reduce CO_2 emission linked to climate change. It is a sustainable clean energy source if produced using renewable energy resources rather than through fossil fuels. For H_2-based technologies to address our future energy needs, lower cost, more efficient ways of generating hydrogen in a carbon-neutral fashion are needed.[1] One long sought after goal involves photocatalytic hydrogen generation, using sunlight to split water.[2–4]

Efficient photocatalytic hydrogen generation, however, requires that photocatalysts meet certain stringent criteria. Namely, their conduction (E_{CB}) and valence bands (E_{VB}) must possess appropriate electrochemical potentials ($E_{CB} \leq -0.41$ V and $E_{VB} \geq +0.82$ V versus normal hydrogen electrode at pH = 7). Furthermore, the catalyst's band gap (E_g) must be ideally positioned within the visible part of the solar spectrum where sunlight is most intense (i.e. E_g ~1.7-3.1 eV). Long carrier lifetimes are also needed to ensure that desired chemical reactions effectively compete with native photocatalyst charge recombination processes.

Semiconductor nanostructures are promising systems for photocatalytic hydrogen generation.[4–8] As examples, CdSe nanobelts (NBs)[5] and quantum dots (QDs)[6] suspended in aqueous solutions of hole-scavengers actively produce H_2 under visible light irradiation with rates of ~0.44 and ~1.15 mmol h^{-1} g^{-1}, respectively. By contrast, bulk CdSe is inactive as a photocatalyst.[9]

Additional advantages of nanoscale materials include the ease by which their chemical, physical, optical and electrical properties can be tailored through size-, shape- and dimensionality. Nanostructure hydrogen generation efficiencies can also be enhanced by implementing nanoscale semiconductor/semiconductor heterointerfaces.[10,11] Such junctions significantly increase carrier lifetimes and enhance H_2 generation rates. For example, 10-fold photocatalytic hydrogen generation rate enhancements have been reported for CdSe QDs overcoated with CdS (~10.39 mmol h^{-1} g^{-1}).[7] Analogous enhancements have been observed for dot-in-rod nanostructures such as CdSe QDs embedded in CdS nanorods (NRs).[8]

Adding to abovementioned systems, nanostructures which feature metal/semiconductor heterojunctions (e.g. with noble metals such as Pt or Pd) possess enhanced photocatalytic hydrogen generation activities.[12–17] This is because in many cases metal co-catalysts act as acceptors for photogenerated electrons[15,17–19] and simultaneously possess suitable proton binding energies.[20,21] In the specific case of Pt, its low H^+ chemisorption energies make it a particularly effective co-catalyst for hydrogen generation. Supporting this, Pt nanoparticle (NP) decorated CdS NRs have recently shown improved H_2 generation rates of ~ 5 mmol h^{-1} g^{-1}.[14]

In a previous study[22], we have described strategies for producing nanowire-based photocatalysts, containing both semiconductor/semiconductor and metal/semiconductor heterojunctions. These materials were created to explore the effects of introducing such heterointerfaces on nanowire H_2 generation efficiencies. The four systems studied were CdSe NWs, CdSe/CdS core/shell NWs, and their Au NP decorated counterparts. Resulting hydrogen generation efficiencies were found to increase in the order: CdSe < CdSe/Au NP < CdSe/CdS/Au NP < CdSe/CdS NWs with the largest H_2 generation rates found for CdSe/CdS core/shell NWs. Adding Au NPs to either CdSe or CdSe/CdS NWs led to no systematic enhancement of their H_2 generation efficiencies. This suggests that Au NPs might not be an active co-catalyst for hydrogen generation, despite studies which claim small Au NPs to be highly catalytically active[23] or even responsible for plasmonic enhancements of catalytic efficiencies.[24,25]

In this study, we synthesize CdSe nanowire-based photocatalysts which incorporate Pt nanoparticles. This is motivated by the fact that Pt possesses attractive properties for carrying out photocatalytic reactions when compared to other metal co-catalysts.[8,14,17] Namely, a combination of three factors makes Pt NPs optimal for H_2 photogeneration: (i) when placed in direct contact with photoexcited semiconductors, Pt NPs behave as electron sinks;[15,17,18] (ii) electrons acquired by Pt subsequently discharge to surface adsorbed species due to Pt's low electrochemical impedance;[18,26] (iii) favorable proton binding energies make Pt highly active for proton reduction reactions.[3]

In what follows, we use hydrogen evolution tests in concert with spectroscopic transient differential absorption (TDA) measurements to investigate how CdS, CdSe and Pt interact within Pt NP decorated CdSe and CdSe/CdS NWs during photocatalytic hydrogen generation reactions. Electron transfer events across both semiconductor/semiconductor and metal/semiconductor heterojunctions are followed to identify where H_2 is evolved and the role each heterojunction plays in determining a system's overall efficiency.

Results and Discussion

Preparation of materials

CdSe and CdS NWs were synthesized using Solution-Liquid-Solid (SLS) growth.[27–30] Resulting CdSe and CdS NWs were crystalline with mean diameters of 14±2.4 nm and 12±1.5 nm, respectively; lengths exceeded 10 μm in each case. Mean diameters and standard deviations were determined by sizing 100 separate nanowires for both CdSe and CdS. Details about the synthesis along with low and high magnification TEM micrographs of obtained CdSe (**Fig. S1a-b**†) and CdS (**Fig. S1c-d**†) NWs can be found in the Electronic Supplementary Information† (ESI†).

CdSe NWs were subsequently overcoated with CdS to create core/shell NWs.[31–33] Resulting wires consist of a CdSe core surrounded by a ~5 nm shell of CdS nanoparticles. Corresponding low and high magnification TEM images of the wires are provided in **Fig. S2**†. Additional details about the synthesis of core/shell nanowires can be found in the ESI†.

CdS, CdSe, and CdSe/CdS core/shell NWs were decorated with Pt NPs using a thermal deposition approach.[34,35] The process entails mixing a NW suspension in dichlorobenzene (approximate conc. ~1.44×10^{-10} M for all NW samples) with $Pt(acac)_2$ [(10 mg, 0.025 mmol)] and leaving it to stir overnight. CdSe NW concentrations were estimated by assuming a mean diameter of 14 nm, a ~10 μm length and a molar extinction coefficient of $\varepsilon_{650\ nm} = 2.34 \times 10^{10}$ $M^{-1}cm^{-1}$. CdS NW concentrations were similarly estimated using a mean diameter of 12 nm, a 10 μm length and a molar extinction coefficient of $\varepsilon_{480\ nm} = 3.10 \times 10^{10}$ $M^{-1}cm^{-1}$. All extinction coefficients were obtained from model expressions for NW absorption cross sections.[33,36] Details about these concentration estimates can be found in ESI†.

To initiate Pt NP deposition, NW mixtures were injected into a solution of diphenyl ether, oleylamine and oleic acid at 200 °C under N_2. The subsequent reaction was stopped after seven minutes to obtain wires coated with ~3-5 nm diameter Pt NPs. Notably, Pt nanoparticles of this size are highly active co-catalysts for photocatalytic H_2 generation as demonstrated by H_2 generation rates of ~40 mmol $h^{-1}g^{-1}$ obtained from 3 nm Pt NP-tipped CdSe/CdS dot-in-rod heterostructures.[14,17] Additional details about the Pt NP decoration can be found in the ESI†.

To ensure subsequent comparability between samples, nanowire solutions of identical concentration, quality and size distribution were studied. In practice, this involved preparing a large CdSe NW ensemble from which all samples were derived. Specifically, half of a given CdSe NW stock was overcoated with CdS. Resulting core and core/shell nanowire suspensions were then split into two equal parts, half of which was decorated with Pt. In this fashion, four NW solutions were obtained: CdSe NWs, Pt NP decorated CdSe NWs (CdSe/Pt NP), CdSe/CdS core/shell NWs, and Pt NP decorated core/shell wires (CdSe/CdS/Pt NP). Additional CdS NWs and their Pt NP decorated counterparts (CdS/Pt NP) were made as controls. In all cases, Pt loading in samples was adjusted to maintain the Pt NP surface area exposed to reactants approximately equal. The total estimated surface area of Pt in these samples differed by less than 8%. Details of Pt loading adjustment are provided in ESI† (**Fig. S6**).

Low and high magnification TEM images of all three metal/semiconductor hybrid systems: CdS/Pt NP, CdSe/Pt NP, and CdSe/CdS/Pt NP NWs are shown in Fig. 1 as well as in Fig. S3-S5†.

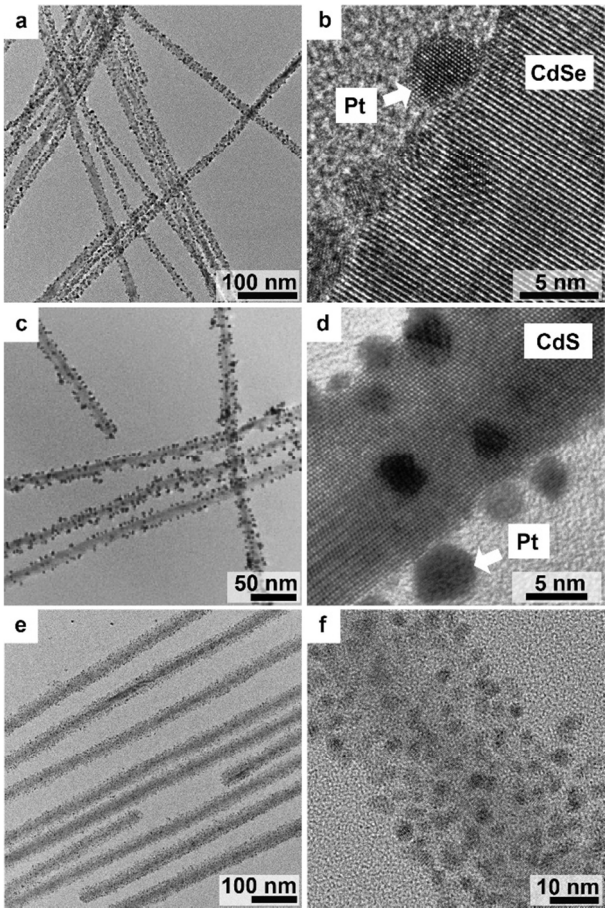

Fig. 1 Low and high magnification TEM images of Pt NP decorated (a-b) CdSe, (c-d) CdS and (e-f) CdSe/CdS core/shell NWs.

Correlated H_2 generation efficiency and transient differential absorption measurements

All NW samples were tested for their photocatalytic H_2 generation activities using two excitation sources. The first involved broadband UV/Visible excitation from a 450 W Xe arc lamp ($\lambda_{exc} \geq 320$ nm, 0.01 M $CuSO_4$ filter). With this source, both the CdSe core and the CdS shell (where present) were excited given their respective band edges of 683 nm (1.82 eV) and 450 nm (2.76 eV). **Fig. S7**† shows the spectral profile of the Xe arc lamp following the $CuSO_4$ filter. The second excitation source was a high power 520 nm green light emitting diode (LED, 200 mW) that selectively excited CdSe but not CdS. By comparing the response of each system under these two excitation conditions, we separately probed the role of a CdS shell in determining the performance of NW-based photocatalysts.

All experiments were conducted by irradiating NW suspensions for 15 hours in aqueous solutions of 0.1 M Na_2S and 0.1 M Na_2SO_3 (1:1 ratio). Large sample optical densities were used to prevent any possible absorption changes during irradiation from influencing observed hydrogen generation yields. Additional details of the photocatalytic H_2 generation measurements can be found in the ESI†. A summary of H_2 generation rates from both broadband (solid blue bars) and 520 nm (shaded red bars) excitation experiments is shown in **Fig. 2**.

We find that bare CdSe NWs under broadband illumination possess an estimated H_2 generation rate of ~1.76 ± 0.48 μmol h^{-1} g^{-1}. This value agrees with that found in our previous study, 1.98 ± 0.55 μmol h^{-1} g^{-1}.[22] Under 520 nm LED excitation, bare CdSe NWs show a lower H_2 generation rate of ~0.30 ± 0.08 μmol h^{-1} g^{-1}. The apparent difference in rates stems from the different number of photons absorbed by the wires in the broadband versus 520 nm experiment. As an illustration, the product of the absorption cross section at 520 nm ($\sigma_{520\ nm}$=1.85 × 10^{-11} cm^2 μm^{-1}) with the 520 nm, incident power 200 mW (photon flux = 5.25 × 10^{17} s^{-1}) yields a photon absorption rate of 9.71 × 10^6 cm^2 μm^{-1} s^{-1}. The analogous product of the integrated broadband cross section (σ_{broad}~1.30 × 10^{-8} cm^2 μm^{-1}) and the white light incident power (11.7 W) gives a broadband photon absorption rate of 5.48 × 10^8 cm^2 μm^{-1} s^{-1}. This latter value is ~50 times larger than the corresponding 520 nm rate and consequently rationalizes observed differences in H_2 generation rates. Additional information about the estimate can be found in the ESI†.

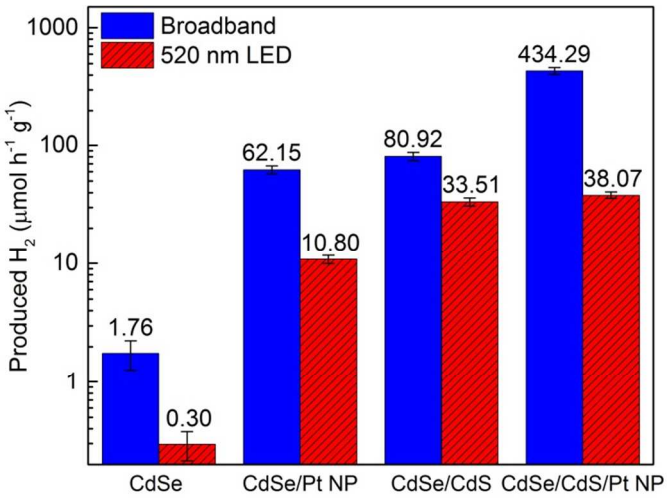

Fig. 2 Photocatalytic H_2 generation rates of CdSe, CdSe/CdS core/shell NWs and their Pt NP decorated counterparts in aqueous solutions of Na_2S and Na_2SO_3 under broadband (solid blue bars) and 520 nm (shaded red bars) excitation.

In either experiment, low overall H_2 generation efficiencies stem from the unfavorable competition that exists with native charge recombination processes in bare CdSe NWs. This is demonstrated using femtosecond TDA experiments. Details of the TDA experiments can be found in the ESI†. In this regard, transient differential absorption spectroscopy is an important tool for probing the photophysics of semiconductor nanostructures because it allows one to spectroscopically follow the kinetics of excited carriers.[37] For II-VI materials such as CdS and CdSe, observed TDA bleaches reflect the population of excited conduction band electrons given their

smaller effective mass relative to those of corresponding holes.[37] Thus, by monitoring the temporal evolution of TDA bleaches, electron transfer reactions in II-VI nanostructures as well as their kinetics can be studied.

Fig. 3a shows both the linear absorption (top) and corresponding transient differential absorption spectrum (bottom) of CdSe NWs taken 4.4 ps after excitation (λ_{exc}=387 nm). A bleach is observed at 683 nm and correlates well with the absorption edge of the wires. The associated maximum fractional absorption change is $|\Delta A|/A = 0.599$ and shows that most of the excited charge carriers relax to the CdSe band edge. A bleach is also seen at 560 nm and is associated with the CdSe split off transition.[38] Corresponding TDA spectra of control CdS NW specimens are shown in **Fig. S8**†.

By following the temporal evolution of CdSe's TDA bleaches, we find characteristic timescales for charge relaxation and recombination in this system. Specifically, exponential fits to the band edge bleach growth show that intraband relaxation within CdSe NWs occurs with a ~1.45 ps time constant. This agrees with prior results acquired on CdSe NWs and nanorods, showing intraband relaxation timescales ranging from 0.6 - 3 ps.[33,39,40] The rise of the CdSe NW band edge bleach and its associated kinetic fit can be found in **Fig. S9**†.

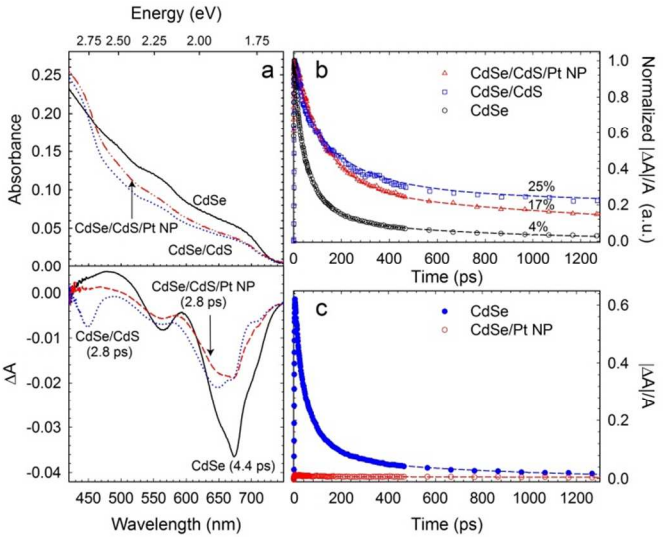

Fig. 3 (a) Linear absorption spectra (top panel) of CdSe, CdSe/CdS and CdSe/CdS/Pt NP NWs as well as their corresponding (λ_{exc} = 387 nm) TDA spectra (bottom panel). Numbers in parentheses indicate when TDA spectra were acquired. (b) Comparison of CdSe, CdSe/CdS and CdSe/CdS/Pt NP NW band edge bleach kinetics when excited at λ_{exc} = 387 nm. (c) Comparison of CdSe and CdSe/Pt NP NW band edge bleach kinetics when excited at λ_{exc} = 387 nm.

Subsequent decay of the band edge bleach (**Fig. 3b**) reveals three distinct relaxation timescales. Namely, triexponential fits to the data show a 23 ps component (43% contribution), a 91 ps component (45% contribution) and a longer 791 ps component (12% contribution). The two fast components likely reflect rapid nonradiative recombination in the NWs.[41] It may also reflect Auger processes, especially when carrier densities are large.[39,42–44] For the d=14 nm CdSe nanowires studied, an estimate using an absorption cross section[33,36] of $\sigma_{387nm} = 4.07 \times 10^{-11}$ cm^2 μm^{-1} and a 20 μJ cm^{-2} pump fluence, results in an initial e-h carrier density [$n(0)$] of 1.0×10^{19} cm^{-3} [$n(0)=j\sigma/h\nu V$, where j is the pump fluence, $h\nu$ is the 387 nm photon energy, and V is the nanowire volume]. This initial carrier density is on the low end of reported bimolecular and three-carrier Auger recombination thresholds [$n(0) > 10^{19}$ cm^{-3}, and $n(0) \sim 7 \times 10^{18}$ cm^{-3}, respectively]. Consequently, Auger effects are not considered in what follows.

The long 791 ps decay reflects slow electron trapping into defect states.[41] Fits to the TDA kinetics show that CdSe NWs retain ~4% of their initial bleach signal at 1 ns (**Fig. 3b**). This is consistent with previous TDA results on bare CdSe NWs where an 8% retention of the initial bleach magnitude was found at 1 ns.[22] These long lived charges are of relevance to photocatalysis since they are likely responsible for the reduction chemistries of interest. However, the data clearly shows that the majority of initially photogenerated carriers recombine nonradiatively. We therefore conclude that fast nonradiative recombination decreases the number of long-lived electrons, capable of carrying out desired reduction chemistries. As a consequence, low overall photocatalytic efficiencies result.

Next, we have analyzed the H_2 generation efficiencies of CdSe/CdS core/shell NWs. We find a significant increase in activity under broadband excitation. A corresponding H_2 generation rate of ~80.92 ± 6.52 μmol h^{-1} g^{-1} is found, which is ~46 times larger than the performance of bare CdSe NWs (**Fig. 2**). This agrees with our previous study where we found a CdSe/CdS NW H_2 generation rate of 58.06 ± 3.59 μmol h^{-1} g^{-1}.[22] Differences from our previous result likely stem from batch-to-batch variations of NW structural defects. The trend holds when selectively exciting the CdSe core with 520 nm light. Under these conditions, CdSe/CdS NWs exhibit a H_2 generation rate of ~33.51 ± 2.63 μmol h^{-1} g^{-1}. This is ~100 times larger than the efficiency of bare CdSe NWs under the same conditions.

We attribute these enhancements to increased carrier lifetimes that result from improvements to the nanowire surface passivation by adding a CdS shell. The porous CdS shell partially covers CdSe and compensates for surface dangling bonds that can act as charge trapping/charge recombination sites.[22] Suppression of non-radiative charge recombination via shell passivation is supported by photoluminescence quantum yield (QY) increases of CdSe/CdS core/shell NWs compared to their bare CdSe NW counterparts as previously reported by Goebl et al.[33] and Li et al.[31] In the latter study, CdSe NWs coated with 6 (10) monolayers of CdS possess a QY of 0.25% (0.46%), a 79% (229%) increase in efficiency over that of bare CdSe NWs (0.14%).

The conclusion is also supported by corresponding TDA measurements (λ_{exc} = 387 nm) where sizable enhancements of band edge carrier lifetimes are observed. Specifically, **Fig. 3a** shows the TDA spectrum of core/shell wires, which exhibits two bleaches, one at ~450 nm and a second at ~683 nm

(maximum |ΔA|/A = 0.391). The former stems from carriers in CdS while the latter arises due to carriers that have relaxed to the CdSe conduction band edge. Based on a comparison to the maximum band edge bleach |ΔA|/A of bare CdSe nanowires (|ΔA|/A = 0.599), we conclude that a comparable band edge charge density is generated in CdSe/CdS nanowires. The rise time associated with the core CdSe bleach is ~1.32 ps, which is near identical to that observed in bare CdSe NWs (~1.45 ps). This indicates that intraband relaxation in CdSe does not change significantly upon overcoating it with CdS.

By subsequently following the (λ_{exc} = 387 nm) band edge bleach recovery kinetics of the CdSe core, we find two distinct relaxation timescales. Namely, biexponential fits to the data show a fast 101 ps component (60% contribution) as well as a slow 2.04 ns component (40% contribution). When compared to the bare CdSe NW bleach recoveries discussed earlier, we find that slow component lifetimes increase as well as their relative weights. This trend is maintained when only the core is excited using a 560 nm pump. Specifically, a triexponential (best) fit to the resulting decay yields decay contributions of 36 ps (27% contribution), 180 ps (54% contribution) and 15.14 ns (19 % contribution), revealing a sizable long timescale tail (see **Fig. S10**†).

From a photocatalytic standpoint, what is important is that the fraction of long lived charges in the CdSe core at 1 ns increases to ~25% (λ_{exc} = 387 nm, **Fig. 3b**) [19% (λ_{exc} = 560 nm)]. This is again consistent with TDA results from our previous study, which showed a similar long-lived charge fraction at 1 ns [33% (λ_{exc} = 387 nm); 16% (λ_{exc} = 560 nm)].[22] Consequently, we conclude that increased electron lifetimes in core/shell NWs primarily stem from improvements to the surface passivation of CdSe. This, in turn, removes competing non-radiative charge recombination pathways and helps rationalize improved CdSe/CdS NW H_2 generation rates. In this regard, given that **Fig. 2** shows that H_2 generation rates do not change significantly when core/shell wires are excited with broadband or 520 nm light, we conclude that a sizable fraction of the reduction chemistry occurs at the CdSe core. This is aided by the above long carrier lifetimes and by the fact that the nanocrystalline CdS shell is porous.[22]

Having established the kinetic timescales underlying charge relaxation/recombination in CdSe and CdSe/CdS NWs, we now investigate the performance of both core and core/shell species upon introducing a metal/semiconductor heterojunction. In the case of CdSe/Pt NP NWs, we find that both their broadband (62.15 ± 4.88 μmol h^{-1} g^{-1}) and selective 520 nm (10.80 ± 0.87 μmol h^{-1} g^{-1}) H_2 generation rates improve ~35- and 36-fold respectively relative to those of bare CdSe NWs. These observed enhancements also agree with literature reports which show Pt NP decorated CdSe NRs and QDs to exhibit noticeably improved H_2 generation rates compared to their undecorated counterparts.[4,3,14,17] This should be contrasted to the case of CdSe/Au NP NWs where no apparent improvement in H_2 generation rates was observed.[22] The difference in response can be attributed to the favorable H^+ binding energies as well as fast electron discharge kinetics of Pt.[18,26] This is further corroborated by the results of Bang et al. where CdSe/Pt NP decorated NRs exhibited ~44 fold better H_2 generation rates over their Au NP decorated counterparts.[26]

To link the performance of CdSe/Pt NP NWs with their underlying photophysics and to better establish the role played by Pt, we again conduct TDA spectroscopy. In the case where the metal of interest possesses a visible plasmon resonance, TDA can directly report on electron transfer events at the metal/semiconductor interface. As an example, Au's plasmon resonance at ~530 nm is sensitive to both thermal effects as well as charge injection and has been used to characterize femtosecond charge transfer dynamics in Au-tipped CdS NRs.[13,42]

Pt NPs, by contrast, possess no visible plasmon resonance. As a consequence, charge transfer to Pt in CdSe/Pt NP NWs must be deduced indirectly through a significant shortening of the semiconductor band edge bleach recovery. This reflects the introduction of rapid charge transfer pathways to the metal that compete with native charge recombination processes in CdSe.

In the current study, the (λ_{exc} = 387 nm) TDA band edge bleach growth and its subsequent recovery occur very quickly compared to bare CdSe wires (**Fig. 3c**). Specifically, we find a sub picosecond rise time (τ<<1 ps) followed by a fast bleach recovery that approaches the instrument's temporal response function (~180 fs). What results is a near zero CdSe band edge bleach magnitude (maximum |ΔA|/A = 0.012) (see **Fig. S11**†). As a point of reference, maximum |ΔA|/A values in CdSe and CdSe/CdS NWs were previously seen to be 0.599 and 0.391. We also find no residual bleach at 1 ns, indicating complete extraction of electrons from the semiconductor. An identical result is observed when exciting at 560 nm (maximum |ΔA|/A = 0.021) (see **Fig. S11**†). Relaxation processes associated with the introduction of Pt therefore have timescales competitive with carrier cooling in CdSe (0.6-3 ps timescale).[33,39] This suggests possible hot electron transfer to Pt NPs, as previously reported for CdS/Pt NP NRs,[15] CdSe/Pt NP NRs,[45] and Pt/CdSe/Pt nanodumbbells.[13,43]

Another fast relaxation process that possibly accounts for ultrafast charge relaxation in CdSe/Pt NP NWs involves energy transfer from CdSe to Pt. Although the literature suggests that this is not a significant relaxation pathway,[42] H_2 generation measurements enable us to directly test the role energy transfer plays within CdSe/Pt NP NWs. In particular, given that Pt is an efficient hydrogen generating co-catalyst,[3] any charge transfer to it will increase NW photocatalytic hydrogen generation efficiencies. By contrast, energy transfer is an exclusive carrier loss mechanism that suppresses hydrogen evolution. As a consequence, lower H_2 generation rates for Pt NP decorated NWs should result if energy transfer dominates.

Experimentally, we see a strong enhancement of H_2 generation rates in CdSe/Pt NP NWs under both broadband (62.15 ± 4.88 μmol h^{-1} g^{-1}, a 35-fold improvement over bare CdSe NWs) and 520 nm excitation (10.80 ± 0.87 μmol h^{-1} g^{-1}, a 36-fold improvement over bare CdSe NWs). The same is true of control CdS/Pt NP NWs under broadband excitation (170.59 ± 15.53 μmol h^{-1} g^{-1}, a 5-fold improvement over bare CdS

NWs, **Fig. S12**†). These results therefore suggest that ultrafast charge transfer from CdSe (or CdS) to Pt is the dominant interaction across the metal/semiconductor heterojunction in these hybrid systems and that efficient H_2 generation occurs at the Pt NP/solvent interface.

At this point, we investigate the performance of CdSe/CdS/Pt NP NWs, a double heterojunction system consisting of a CdSe/CdS and a CdS/Pt interface. In principle, this system combines the advantages of both semiconductor/semiconductor and metal/semiconductor heterojunctions in terms of enhanced carrier lifetimes and the presence of a suitable catalytically active metal. In the experiment, we find that CdSe/CdS/Pt NP NWs exhibit a broadband H_2 generation rate of ~434.29 ± 27.40 μmol h^{-1} g^{-1}, which is a 7-fold improvement over CdSe/Pt NP NWs, a 5-fold improvement over the performance of CdSe/CdS core/shell wires, and a ~240-fold improvement over that of bare CdSe NWs. Interestingly, the associated 520 nm H_2 generation rate (~38.07 ± 2.40 μmol h^{-1} g^{-1}) is comparable to that of CdSe/CdS NWs (~33.51 ± 2.63 μmol h^{-1} g^{-1}).

We subsequently probe the underlying photophysics of CdSe/CdS/Pt NP NWs using TDA measurements to monitor the flow and accumulation of electrons across the two interfaces present. These experiments show differences as well as similarities in the (λ_{exc} = 387 nm) TDA response of CdSe/CdS/Pt NP NWs relative to those of CdS, CdSe, CdSe/Pt NP and CdSe/CdS NWs. First, no bleach from the CdS shell is observed unlike the case of CdSe/CdS NWs (**Fig. 3a**). Next, the observed CdSe core band edge bleach magnitude (maximum |ΔA|/A ~0.448) is comparable to that of either bare CdSe or CdSe/CdS NWs under 387 nm excitation. Moreover, it grows in over near identical timescales (~1.49 ps), unlike the response of CdSe/Pt NP NWs.

Subsequent analysis of the CdSe band edge bleach recovery shows rate constants similar to those of CdSe/CdS nanowires. Specifically, biexponential fits reveal a fast 130 ps component (72% contribution) and a slow 1.92 ns component (28% contribution). Corresponding analysis of the λ_{exc} = 560 nm decay reveals (best fit) triexponential decay components similar to those seen earlier in core/shell NWs: 62 ps (67% contribution), 331 ps (21% contribution) and 4.44 ns (12% contribution) (see **Fig. S13**†). Long-lived charges are therefore present within the CdSe core, resulting in charge fractions of 17% (λ_{exc} = 387 nm, **Fig. 3b**) and 11% (λ_{exc} = 560 nm, **Fig. S13**†) at 1 ns.

The above rate constants are summarized in **Fig. 4** which shows a kinetic model, constructed from rate constants extracted from CdS, CdS/Pt NP, CdSe, CdSe/Pt NP, CdSe/CdS, and CdSe/CdS/Pt NP NW TDA results. Using the model, we qualitatively explain the above observations as well as the overall performance of CdSe/CdS/Pt NP NWs as a H_2 generation photocatalyst. First, we establish that based on absorption alone (whether broadband or 520 nm excitation) sizable difference in H_2 generation rates should not exist between CdSe, CdSe/Pt NP, CdSe/CdS and CdSe/CdS/Pt NP NWs. Qualitatively, CdSe is the dominant absorber in all cases. Additional details about these absorption rate estimates can be found in the ESI†. As a consequence, large differences in H_2 generation rates between CdSe, CdSe/Pt NP, CdSe/CdS, and CdSe/CdS/Pt NP NWs (**Fig. 2**) must stem from details of the subsequent charge recombination in CdSe/CdS/Pt NP NWs.

In this regard, absence of a CdS bleach suggests lack of a sizable CdS shell electron population due to fast electron transfer into either CdSe or Pt (as previously seen with CdSe/CdS and CdS/Pt NP NWs**, Fig. 4**, processes 1 and 2). However, the similar maximum |ΔA|/A value to that of bare CdSe NWs (|ΔA|/A ~0.448 versus |ΔA|/A ~0.599) suggests that this absence does not stem from charge transfer to CdSe (**Fig. 4**, process 1). Instead, it likely reflects selective electron extraction from CdS into Pt (**Fig. 4**, process 2) and is further corroborated by the much faster overall decay of the CdS band edge bleach in CdS/Pt NP NWs relative to that in core/shell wires (**Fig. S14**†). While energy transfer from CdS into Pt is also possible, we have previously shown that observed increases in broadband H_2 generation rates are more consistent with electron transfer over energy transfer since the latter is an exclusive carrier loss mechanism. Electrons accumulated by Pt are subsequently discharged into the solvent and are used to carry out desired reduction chemistries.

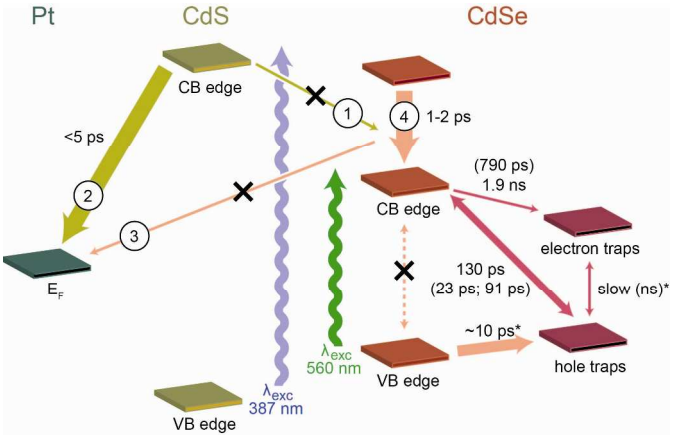

Fig. 4 Schematic showing the relative band alignment of CdS, CdSe and Pt as well as relevant electron transfer processes across the CdSe/CdS/Pt NP double heterojunction. Wavy arrows represent charge generation processes under 387 and 560 nm excitation. Single-ended arrows indicate charge transfer processes while double-headed arrows represent charge recombination processes. Timescales are provided along with corresponding values for bare CdSe (in parentheses). Arrow thicknesses are scaled to represent a given processes' relative kinetic rate. (*) denotes numbers taken from ref. 41.

Next, carriers generated directly in the CdSe core remain unaffected by the presence of Pt. This is due to their spatial separation, which suppresses charge transfer (**Fig. 4**, process 3). Consequently, photogenerated carriers in the core relax to the CdSe band edge on the 1-2 ps timescale as in bare CdSe or CdSe/CdS NWs (**Fig. 4**, process 4). This explains the near identical band edge bleach growth kinetics as well as similar maximum |ΔA|/A values that are observed. Once at the band edge, these carriers experience the same enhanced lifetimes that

stem from the surface passivation of CdSe. In turn, ns timescale band edge bleach recoveries (akin to those seen in CdSe/CdS NWs) result in sizable residual charge fractions at a nanosecond.

The above kinetic model additionally presents simple qualitative predictions that can be tested. Namely, given that CdSe and Pt are spatially separated and do not readily communicate with each other via charge transfer, long-lived carriers should be present in CdSe, irrespective of whether both the core and the shell or just the core in CdSe/CdS/Pt NP NWs are excited. TDA experiments show exactly this, revealing ns timescale decays when NWs are excited at either λ_{exc} = 387 nm or λ_{exc} = 560 nm (**Fig. S13**†). Furthermore, based on the weak interaction between CdSe and Pt, the kinetic model suggests that the H_2 generation efficiencies of CdSe/CdS/Pt NP and CdSe/CdS NWs should be near identical when only the CdSe core is excited. Indeed, **Fig. 2** shows only minor differences in H_2 generation rates between the two systems under 520 nm excitation (CdSe/CdS NWs ~33.51 ± 2.63 μmol h^{-1} g^{-1} vs. CdSe/CdS/Pt NP NWs ~38.07 ± 2.40 μmol h^{-1} g^{-1}).

Finally, the kinetic model addresses Pt's role in improving H_2 generation rates since the selective charge transfer of photogenerated charges from CdS to Pt means that this system effectively behaves as two photocatalysts in one. Namely, the CdS shell passivates CdSe surface defects to enhance carrier lifetimes for charges generated directly in the core. However, it also absorbs light and selectively injects carriers into Pt. Thus, hydrogen is generated at both the Pt NP/solvent and CdSe/CdS interfaces in CdSe/CdS/Pt NP NWs. It follows that the H_2 generation rate of CdSe/CdS/Pt NP NWs should be similar to the sum of those from both CdS/Pt NP and CdSe/CdS NWs. Indeed, Figure 2 shows this, revealing that the H_2 generation rate of CdSe/CdS/Pt NP NWs has the same order of magnitude as the sum of H_2 generation rates from CdS/Pt NP and CdSe/CdS NWs (CdSe/CdS/Pt NP: 434.29 μmol h^{-1} g^{-1}; CdS/Pt NP + CdSe/CdS NW: 251.51 μmol h^{-1} g^{-1}). Differences in the two values could be due to variations in electron injection efficiencies at two structurally different interfaces: namely, the CdS nanowire/Pt NP interface and the interface between a nanocrystalline CdS shell and surface adsorbed Pt NPs.

Conclusions

To summarize, we have conducted a concerted study of the H_2 generation ability and underlying photophysics of several CdSe NW-based photocatalysts. Both single junction (i.e. CdSe/CdS and CdSe/Pt NP) and double junction (i.e. CdSe/CdS/Pt NP) systems have been investigated. From concerted H_2 generation and transient differential absorption experiments, we have established the primary interactions that govern the performance of these multicomponent catalysts. We find that in the single junction case, coating a semiconductor to form core/shell structures is beneficial since this increases carrier lifetimes by reducing the influence of surface defects which act as nonradiative recombination centers. In turn, larger photocatalytic efficiencies result. In double heterojunction systems, electron transfer from the shell to the metal becomes possible and when the metal is catalytically active, as with Pt, sizable increases to the system's H_2 generation efficiency result. Double heterojunction systems therefore enable reduction chemistries to be conducted at not one, but rather two interfaces, taking advantage of each junction's optimal catalytic activities.

Acknowledgements

This research has been supported by the Center for Sustainable Energy at Notre Dame (cSEND). The authors thank the Center's Materials Characterization Facility (MCF), the Notre Dame Integrated Imaging Facility (NDIIF), as well as the Notre Dame Radiation Laboratory/Department of Energy (DOE), Office of Basic Energy Sciences, for use of their facilities and equipment. This is contribution No. NDRL-5006 from the Notre Dame Radiation Laboratory. Use of JEOL JSM-7500F Field Emission-SEM at the Center for Nanoscale Materials was supported by the U. S. Department of Energy, Office of Science, Office of Basic Energy Sciences, under Contract No. DE-AC02-06CH11357. P. Tongying thanks the Royal Thai Government Scholarships for partial financial support and Prof. Prashant V. Kamat for useful discussions.

Notes and references

[a] Department of Chemistry and Biochemistry, University of Notre Dame, 251 Nieuwland Science Hall, Notre Dame, Indiana 46556, United States.
[b] Faculty of Physics, Taras Shevchenko National University of Kiev, 4 Prospect Glushkova, Kiev, 03022 Ukraine.
[c] Notre Dame Radiation Laboratory, University of Notre Dame, 338 Radiation Research Building, Notre Dame, Indiana 46556, United States.
[d] Department of Civil and Environmental Engineering and Earth Sciences, University of Notre Dame, 156 Fitzpatrick Hall, Notre Dame, IN 46556, United States.

*Corresponding authors: gkrylova@nd.edu; mkuno@nd.edu

† Electronic Supplementary Information (ESI) available: [Details of NW syntheses, processing and characterization. Additional TEM images of CdS, CdSe and CdSe/CdS core/shell NWs. NW concentration and cross section estimates. Details of the Pt NP decoration. Additional TEM images of Pt NP decorated CdS, CdSe and CdSe/CdS core/shell NWs. Size distribution of Pt NPs for CdSe/Pt NP and CdSe/CdS/Pt NP NWs. Xe arc lamp spectrum. Details of H_2 generation experiments. Estimated photon absorption rate. Details of TDA measurements. TDA spectra and kinetics of CdS and CdS/Pt NP NWs. Plot illustrating CdSe NW band edge bleach kinetics. Comparison of CdSe band edge bleach kinetics in CdSe/CdS core/shell NWs when excited at λ_{exc} = 387 nm and λ_{exc} = 560 nm. Comparison of CdSe band edge bleach kinetics in CdSe/Pt NP NWs when excited at λ_{exc} = 387 nm and λ_{exc} = 560 nm. Bar graph showing H_2 generation efficiencies of CdS and CdS/Pt NP NWs. Bleach kinetics of CdSe/CdS/Pt NP NWs at λ_{exc} = 387 nm and λ_{exc} = 560 nm. Comparison of CdS band edge bleach kinetics in CdS/Pt NP, and CdSe/CdS core/shell NWs when excited at λ_{exc} = 387 nm.] See DOI: 10.1039/b000000x/

1. N. S. Lewis and D. G. Nocera, *Proc. Natl. Acad. Sci.*, 2006, **103**, 15729–15735.
2. A. J. Esswein and D. G. Nocera, *Chem. Rev.*, 2007, **107**, 4022–4047.
3. F. E. Osterloh, *Chem Mater*, 2008, **20**, 35–54.
4. X. Chen, S. Shen, L. Guo, and S. S. Mao, *Chem Rev*, 2010, **110**, 6503–6570.
5. F. A. Frame, E. C. Carroll, D. S. Larsen, M. Sarahan, N. D. Browning, and F. E. Osterloh, *Chem. Commun.*, 2008, 2206–2208.
6. M. A. Holmes, T. K. Townsend, and F. E. Osterloh, *Chem. Commun.*, 2012, **48**, 371–373.
7. A. Thibert, F. A. Frame, E. Busby, M. A. Holmes, F. E. Osterloh, and D. S. Larsen, *J. Phys. Chem. Lett.*, 2011, **2**, 2688–2694.
8. H. Zhu, N. Song, H. Lv, C. L. Hill, and T. Lian, *J. Am. Chem. Soc.*, 2012, **134**, 11701–11708.
9. S. Kambe, M. Fujii, T. Kawai, S. Kawai, and F. Nakahara, *Chem. Phys. Lett.*, 1984, **109**, 105–109.
10. H. Zhu, N. Song, and T. Lian, *J. Am. Chem. Soc.*, 2010, **132**, 15038–15045.
11. D. Barpuzary, Z. Khan, N. Vinothkumar, M. De, and M. Qureshi, *J Phys Chem C*, 2011, **116**, 150–156.
12. R. Costi, A. E. Saunders, and U. Banin, *Angew. Chem. Int. Ed.*, 2010, **49**, 4878–4897.
13. D. Mongin, E. Shaviv, P. Maioli, A. Crut, U. Banin, N. Del Fatti, and F. Vallée, *ACS Nano*, 2012, **6**, 7034–7043.
14. M. Berr, A. Vaneski, A. S. Susha, J. Rodríguez-Fernández, M. Do□blinger, F. Ja□ckel, A. L. Rogach, and J. Feldmann, *Appl. Phys. Lett.*, 2010, **97**, 093108.
15. K. Wu, H. Zhu, Z. Liu, W. Rodríguez-Córdoba, and T. Lian, *J. Am. Chem. Soc.*, 2012, **134**, 10337–10340.
16. Y. Shemesh, J. E. Macdonald, G. Menagen, and U. Banin, *Angew. Chem.*, 2011, **123**, 1217–1221.
17. L. Amirav and A. P. Alivisatos, *J. Phys. Chem. Lett.*, 2010, **1**, 1051–1054.
18. A. Wood, M. Giersig, and P. Mulvaney, *J Phys Chem B*, 2001, **105**, 8810–8815.
19. K. P. Acharya, R. S. Khnayzer, T. O'Connor, G. Diederich, M. Kirsanova, A. Klinkova, D. Roth, E. Kinder, M. Imboden, and M. Zamkov, *Nano Lett.*, 2011, **11**, 2919–2926.
20. B. E. Conway and B. V. Tilak, *Electrochimica Acta*, 2002, **47**, 3571–3594.
21. J. K. Nørskov, T. Bligaard, A. Logadottir, J. R. Kitchin, J. G. Chen, S. Pandelov, and U. Stimming, *J. Electrochem. Soc.*, 2005, **152**, J23–J26.
22. P. Tongying, V. V. Plashnitsa, N. Petchsang, F. Vietmeyer, G. J. Ferraudi, G. Krylova, and M. Kuno, *J. Phys. Chem. Lett.*, 2012, **3**, 3234–3240.
23. M. Haruta, *Catal. Today*, 1997, **36**, 153–166.
24. S. C. Warren and E. Thimsen, *Energy Env. Sci*, 2011, **5**, 5133–5146.
25. S. Mubeen, J. Lee, N. Singh, S. Krämer, G. D. Stucky, and M. Moskovits, *Nat. Nanotechnol.*, 2013, **8**, 247–251.
26. J. U. Bang, S. J. Lee, J. S. Jang, W. Choi, and H. Song, *J. Phys. Chem. Lett.*, 2012, **3**, 3781–3785.
27. F. Wang, A. Dong, J. Sun, R. Tang, H. Yu, and W. E. Buhro, *Inorg. Chem.*, 2006, **45**, 7511–7521.
28. F. Wang and W. E. Buhro, *Small*, 2010, **6**, 573–581.
29. Z. Li, Ö. Kurtulus, N. Fu, Z. Wang, A. Kornowski, U. Pietsch, and A. Mews, *Adv. Funct. Mater.*, 2009, **19**, 3650–3661.
30. J. Puthussery, T. H. Kosel, and M. Kuno, *Small*, 2009, **5**, 1112–1116.
31. Z. Li, X. Ma, Q. Sun, Z. Wang, J. Liu, Z. Zhu, S. Z. Qiao, S. C. Smith, G. (Max) Lu, and A. Mews, *Eur. J. Inorg. Chem.*, 2010, **2010**, 4325–4331.
32. Y.-H. Liu, F. Wang, J. Hoy, V. L. Wayman, L. K. Steinberg, R. A. Loomis, and W. E. Buhro, *J. Am. Chem. Soc.*, 2012, **134**, 18797–18803.
33. J. A. Goebl, R. W. Black, J. Puthussery, J. Giblin, T. H. Kosel, and M. Kuno, *J. Am. Chem. Soc.*, 2008, **130**, 14822–14833.
34. K. Ahrenstorf, O. Albrecht, H. Heller, A. Kornowski, D. Görlitz, and H. Weller, *Small*, 2007, **3**, 271–274.
35. I. J. Plante, S. E. Habas, B. D. Yuhas, D. J. Gargas, and T. Mokari, *Chem. Mater.*, 2009, **21**, 3662–3667.
36. J. Giblin and M. Kuno, *J. Phys. Chem. Lett.*, 2010, **1**, 3340–3348.
37. V. I. Klimov, *J. Phys. Chem. B*, 2000, **104**, 6112–6123.
38. J. Giblin, F. Vietmeyer, M. P. McDonald, and M. Kuno, *Nano Lett*, 2011, **11**, 3307–3311.
39. I. Robel, B. A. Bunker, P. V. Kamat, and M. Kuno, *Nano Lett.*, 2006, **6**, 1344–1349.
40. M. B. Mohamed, C. Burda, and M. A. El-Sayed, *Nano Lett.*, 2001, **1**, 589–593.
41. F. Vietmeyer, P. A. Frantsuzov, B. Janko, and M. Kuno, *Phys. Rev. B*, 2011, **83**, 115319.
42. K. Wu, W. E. Rodríguez-Córdoba, Y. Yang, and T. Lian, *Nano Lett.*, 2013, **13**, 5255–5263.
43. S. M. Kim, S. J. Lee, S. H. Kim, S. Kwon, K. J. Yee, H. Song, G. A. Somorjai, and J. Y. Park, *Nano Lett.*, 2013, **13**, 1352–1358.
44. Z.-J. Jiang and D. F. Kelley, *J. Phys. Chem. C*, 2010, **114**, 17519–17528.
45. P. Yu, X. Wen, Y.-C. Lee, W.-C. Lee, C.-C. Kang, and J. Tang, *J. Phys. Chem. Lett.*, 2013, 3596–3601.

TOC Figure